第 45 卷 第 1 期
2024 年 1 月
焊 接 学 报
TRANSACTIONS OF THE CHINA WELDING INSTITUTION
Vol. 45(1):58 − 63
January 2024

窄间隙 P-GMAW 仰焊位置熔滴过渡影响因素及控制方法

刘文吉， 肖宇， 杨嘉昇， 朱鹏飞
(天津工业大学, 天津, 300387)

摘要: 管道窄间隙全位置焊接过程中, 在接近仰焊位置容易出现焊接缺陷, 制约了管道施工的质量和效率. 文中针对管道自动焊仰焊位置成形差、可靠性低的问题, 分析 P-GMAW 过程送丝速度、弧长修正、导电嘴到熔池距离等因素对熔滴过渡的影响规律. 结果表明, 增加弧长修正系数可以增大电弧对侧壁的热输入, 能够缓解侧壁熔合不良的问题, 但会使熔滴过渡路径难以控制. 因此当焊枪运动到仰焊位置时, 提高送丝速度有利于获得更小的熔滴、更高的过渡频率; 降低导电嘴到熔池距离, 可以增加电磁力、减小熔滴尺寸, 从而更有利于仰焊位置熔滴向熔池的过渡, 研究结果对于管道窄间隙焊接的工艺设计具有一定的指导意义.

创新点: 获得了管道窄间隙全位置 P-GMAW 过程中, 参数对熔滴过渡的影响规律和控制焊接参数获得更好熔滴过渡的方法.

关键词: 熔滴过渡; 摆动电弧; 熔化极气体保护焊; 窄间隙焊接
中图分类号: TG 441　　**文献标识码:** A　　**doi:** 10. 12073/j. hjxb. 20221212001

0 序言

随着人们对石油天然气的需求急剧增加, 长输管道工程已经成为继铁路、公路、航空和水运之后的第五大运输业[1]. 在石油和天然气的输送管道焊接施工过程中, 采用窄间隙坡口可以减少焊丝填充量, 降低热输入, 具有热输入低、热影响区窄、热变形小、焊缝组织和性能好[2-4] 等优点, 可以满足管道工程高效率和高质量的要求.

管道施工时, 在仰焊位置容易出现两种缺陷: 一是由于坡口角度小, 电弧难以对侧壁加热, 容易出现侧壁未熔合缺陷; 二是熔池在重力的影响下形成中间高两侧低的凸型焊缝, 在多层多道焊接过程中, 凸型的焊缝容易造成层间未熔合的缺陷[5-8]. 为了克服上述缺陷, 徐望辉等人[9] 分析了工艺参数对熔滴过渡的影响, 研究了摆动参数对 GMAW 窄间隙焊接熔池成形的影响; 王定洲等人[10] 分析了焊接位置对熔滴过渡的影响, 发现相同工艺条件下, 随着焊接位置由平焊向仰焊变化, 熔滴过渡频率逐渐降低, 熔滴半径逐渐变大; Alireza 等人[11] 对管道全位置焊接过程中熔滴过渡规律进行了深入地研究, 发现改变电流大小可以调节电弧力, 抵消因重力的变化对熔滴过渡的影响, 改善焊缝成形, 但是单纯改变焊接电流会使焊接热输入发生变化, 需要在焊接电流改变的同时改变焊接电压.

在管道窄间隙焊接过程中, 焊接小车运动到仰焊位置时需要通过增加摆幅、压低焊枪、减小电流、降低焊接速度等工艺调整来保证侧壁熔合和良好的成形, 各个参数的调整需要大量的工艺试验来确定, 要依靠十分有经验的焊工, 耗费人力物力. 文中针对管道窄间隙仰焊位置成形差、缺陷多的问题, 研究弧长修正系数、送丝速度、焊丝端部到工件的距离 (contact tip to workpiece distance, CTWD) 对熔滴过渡的影响规律, 并分析这些参数影响熔滴过渡和焊缝成形的原因, 为优化摆动电弧窄间隙仰焊的焊接工艺提供依据.

1 试验方法

试验材料选用厚度为 15 mm 的 Q235 板材, 试件规格 400 mm × 40 mm × 15 mm, 加工成 16°坡

收稿日期: 2022 − 12 − 12
基金项目: 国家自然科学基金资助项目 (51975410)

口，坡口底部垫一个 3 mm 厚底板如图 1 所示，焊丝采用直径 ϕ 为 1 mm 的低合金钢焊丝，焊前对坡口侧壁、底板进行打磨，去除铁锈、有机物及杂质，焊枪内的保护气体为 80%Ar + 20%CO_2 的富氩混合气，保护气体流量为 15 L/min.

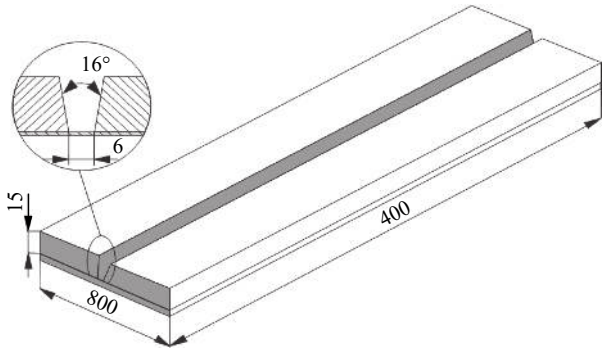

图 1　试件与坡口尺寸示意图 (mm)

Fig. 1　Schematic diagram of test piece and groove

焊接电源采用福尼斯 TPS 3200 焊机，选择脉冲焊模式，焊接参数一元化调节，送丝机采用具有矫正功能的 VR 7000 送丝机，焊接过程中通过数据采集卡实时采集焊接电压和电流，通过高速摄像同步拍摄焊接电弧以及熔滴过渡的图像信息. 高速摄像的采集帧数为 4 000 帧/s，图像处理均采用 imageJ 软件，五点至六点钟位置焊接过程最不稳定，因此将工件摆放成与水平面成 30°，焊接装置示意图如图 2 所示.

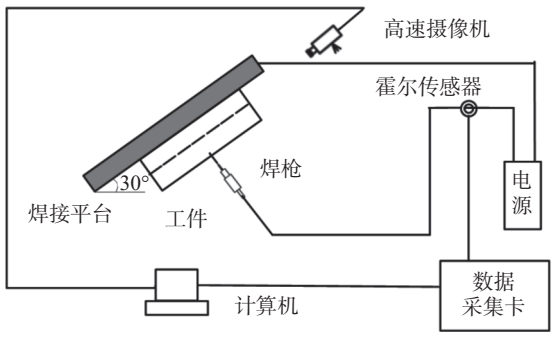

图 2　焊接装置示意图

Fig. 2　Schematic diagram of welding device

试验所用的焊接工艺参数为送丝速度 5 ~ 7 m/min，摆动幅度 3 mm，焊接速度 3.0 mm/s，侧停时间 200 ms，摆动频率 1.5 Hz，弧长修正系数−6 ~ +6，试验过程中只对单一变量进行修改.

2　试验结果与分析

2.1　弧长修正系数对熔滴过渡落点位置的影响

调节弧长修正系数就是在焊机专家系统允许的范围内调节电压，窄间隙坡口的面角度小，坡口侧壁与焊丝轴线几乎平行，当电压发生变化时，电弧的燃烧位置和熔滴过渡均表现出与焊接 V 形坡口时不同的特征.

如图 3 所示，当焊枪摆动到侧壁位置时，随着弧长修正系数的增加，电弧在坡口底部与侧壁交界处燃烧并逐渐向上爬升，直到弧长修正系数为 3 时电弧完全在侧壁处燃烧，此时电弧的位置较高，容易产生咬边现象，此时斑点压力在焊丝末端与焊枪所在侧壁之间产生，因此熔滴的过渡方向并不是沿着焊丝轴线，而是成一定的夹角向另一侧壁过渡，随着弧长修正系数的增加，斑点压力产生的位置越来越不稳定，因此熔滴的过渡方向也随弧长修正系数的增加逐渐偏离焊丝轴线，当弧长修正系数增加到 6 时，熔滴的过渡位置基本都在另一侧壁上，焊接过程十分不稳定.

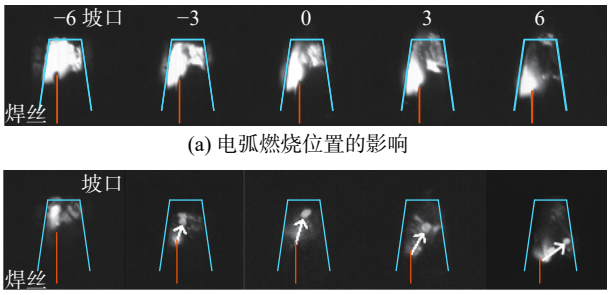

(a) 电弧燃烧位置的影响

(b) 溶滴过渡的影响

图 3　焊枪摆动到侧壁时弧长修正系数对电弧燃烧位置和熔滴过渡路径的影响

Fig. 3　Influence of arc length correction coefficient on arc combustion position and droplet transition path when welding torch swings to side wall. (a) influence on the arc combustion; (b) influence on the droplet transition

为分析熔滴过渡落点的位置，以焊枪所在侧壁与坡口底部的交界处为原点，沿着坡口底部以远离焊枪所在侧壁的方向为正方向建立坐标系如图 4 所示：0 mm 为焊枪所在侧壁与底板的交点处、3 mm 为坡口中心位置、6 mm 为另一侧壁与底板的交点处，当熔滴的过渡位置超过 6 mm 后将会过渡到另一侧侧壁上. 例如，图中 a 熔滴过渡的位置为 2 mm 处，b 熔滴过渡到了对面侧壁上，在坐标轴上的位置为 6.5 mm.

在不同弧长修正系数下进行试验，各记录 20 次熔滴过渡的落点位置，落点分布情况如图 5 所示，从图中可以看出，短路过渡条件下 (修正系数为 −6 时)，熔滴将沿着焊丝轴向过渡到熔池中，熔滴落

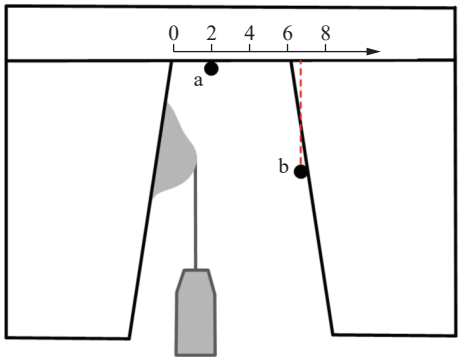

图 4 熔滴过渡位置示意图

Fig. 4 Schematic diagram of droplet transfer position

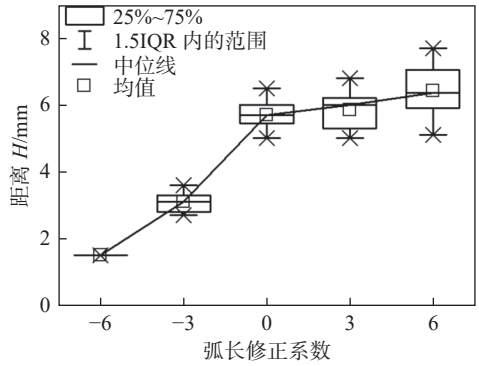

图 5 焊枪在侧壁时不同弧长修正系数下熔滴的过渡位置

Fig. 5 Transfer position of droplet under different arc length correction factors when the welding gun is on the side wall

点的位置十分集中；弧长修正为−3 时，熔滴的过渡位置靠近坡口中心，熔滴落点的范围也很小；弧长修正系数增加到 0 后，大量熔滴过渡到另一侧壁与坡口底部的交界处；弧长修正系数大于 3 之后，不仅熔滴落点的范围增大，而且开始有部分熔滴的过渡到另一侧壁上，熔滴过渡的方向变得越来越不可控.

从上述分析可以看出，当弧长修正系数大于 0 时，窄间隙 P-GMAW 熔滴的落点位置难以控制，会影响焊缝成形，仰焊条件下，采用短弧焊接、短路过渡的方式更容易控制电弧形态和熔池形状，适当的增加弧压 (例如，弧长修正系数增加到 0)，可以形成稳定的滴状无飞溅过渡，但是会使熔滴偏离焊丝轴线，在坡口中心位置形成熔池. 在重力作用下，熔池很难向两侧壁流动，很容易形成中间凸起的焊缝，增加焊后打磨的工作量.

2.2 熔滴受力分析及影响因素分析

2.2.1 熔滴受力分析

仰焊位置焊接，首先要实现熔滴到熔池的稳定过渡，熔滴所受的作用力主要有重力 G、电磁力 F_{em}、等离子流力 F_a 等. 熔滴形成的初始阶段所受到的力如图 6(a) 所示，电磁力和重力均为阻碍熔滴过渡的力，等离子流力为促进熔滴过渡的力，熔滴形成中后期所受到的力如图 6(b) 所示，随着弧根角的增大，电磁力会转化为促进熔滴过渡的力.

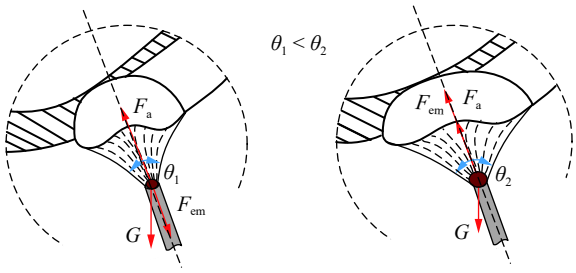

(a) 熔滴初始形成阶段受力 (b) 熔滴形成中后期受力

图 6 熔滴受力示意图

Fig. 6 Diagram of droplet stress.(a) stress in the initial forming stage of droplets; (b) stress in the middle and late stage of droplet formation

熔滴在沿焊丝的轴线方向的重力的分力是阻碍熔滴过渡的力，由于该试验过程中工件与水平面成 30°，其表达式为

$$F_g = \frac{4}{3}\pi R^3 \rho g \cos\frac{\pi}{6} \tag{1}$$

式中：R 为熔滴半径；ρ 为液态熔滴密度；g 为重力加速度. 忽略温度对熔滴密度的影响，假设其为恒定值，则熔滴所受的重力只与它的半径有关，熔滴越小，越有利于过渡.

电磁力对熔滴过渡的影响与弧根角的大小以及焊接电流有关，计算公式如下

$$F_{em} = \frac{\mu_0 I^2}{4\pi}\left[\ln\frac{R\sin\theta}{r} - \frac{1}{1-\cos\theta} + \frac{2}{1-\cos\theta}\ln\frac{2}{1+\cos\theta}\right] \tag{2}$$

式中：I 为焊接电流；μ_0 为自由空间的磁导率；θ 为电弧弧根角；r 为焊丝半径.

如图 7 所示，脉冲初始阶段，弧根角较小、焊接

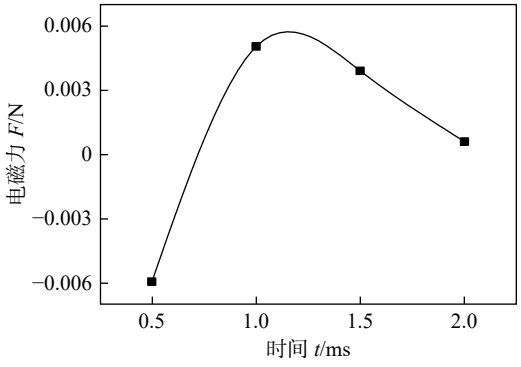

图 7 熔滴过渡前所受的电磁力的变化

Fig. 7 Electromagnetic force before droplet transfer

电流较小，电磁力的计算结果为负，电磁力为阻碍熔滴过渡的力，熔滴不能脱离焊丝，随着焊接电流以及弧根角的增加，熔滴所受电磁力由阻碍熔滴过渡的力逐渐变为促进熔滴过渡的力.

等离子流力会促进熔滴过渡，其表达式为

$$F_a = 0.5\pi v_f \rho_f R^2 C_d \tag{3}$$

式中：v_f为等离子流体速度；ρ_f为等离子流体密度；C_d为阻力系数. 等离子流力始终为促进熔滴过渡的力，当焊接电流增大时，等离子流体速度增加，等离子流力增加，对熔滴的过渡有积极作用.

2.2.2 送丝速度对熔滴过渡频率和直径的影响

在一元化调节模式下，调节送丝速度就是改变焊接电流的大小，不仅影响熔滴过渡频率，而且会影响熔滴直径大小. 送丝速度改变时，熔滴过渡频率和熔滴直径的变化趋势如图 8 所示，从图 8(a) 和图 8(b) 可以看出，随着送丝速度的增加，熔滴过渡频率逐渐增大，熔滴直径逐渐减小；与焊枪在侧壁停留时相比，焊枪运动到坡口中心时的熔滴过渡频率较低，熔滴直径较大.

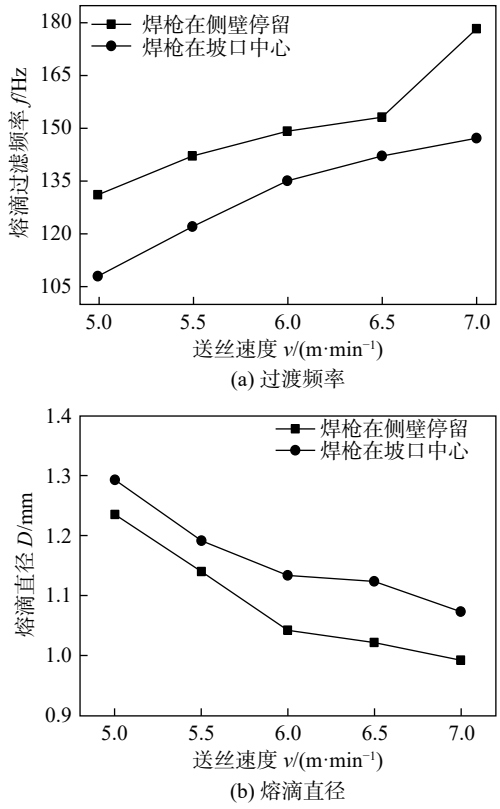

图 8　送丝速度对过渡频率和熔滴直径的影响

Fig. 8　Influence of wire feeding speed on the transition frequenay and droplet diameter. (a) transition frequency; (b) droplet diameter

一脉一滴的情况下，P-GMAW 的熔滴过渡频率取决于脉冲频率如图 9 所示. 观察送丝速度为 5 m/min 和 7 m/min 条件下，焊枪从左侧壁摆动到右侧壁过程中的脉冲频率情况 (每 10 个脉冲计算一次均值)，如图 9(a) 所示. 可以看出，坡口侧壁的脉冲频率高于中心位置的脉冲频率；送丝速度越大，脉冲频率越高，与熔滴过渡频率的变化趋势一致. 这是由于 TPS3200 焊机通过调整脉冲频率来调整热输出，当送丝速度增加时，为了保证焊丝熔化速度与送丝速度平衡，焊机会提高脉冲频率，进而引起熔滴过渡频率升高；当送丝速度不变，焊枪摆动到侧壁时，电弧被压缩，焊机会通过提高脉冲频率来增加热输出，进而加快焊丝熔化，恢复弧长，也会造成熔滴过渡频率的升高.

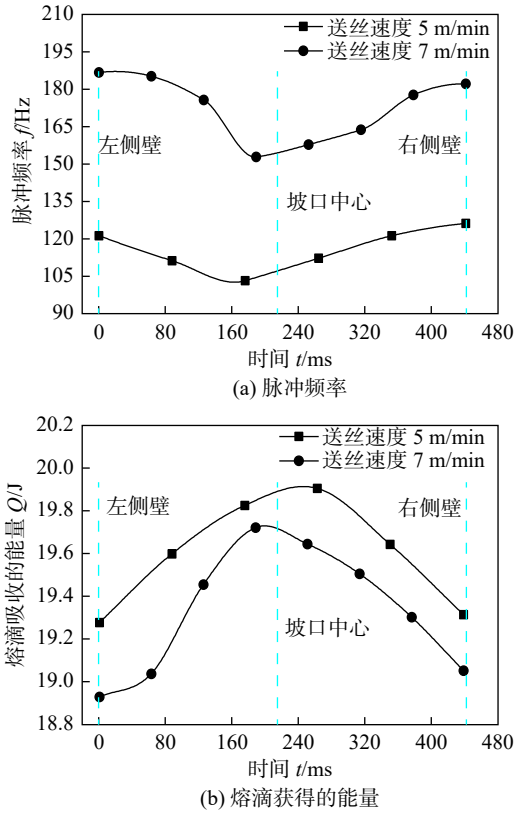

图 9　送丝速度对脉冲频率和熔滴获得的能量的影响

Fig. 9　Influence of wire feeding speed on the pulse frequeney and energy acquisition of moltem droplets. (a) pulse frequency; (b) energy gained by the droplet

而熔滴直径的大小取决于每一个脉冲周期内焊丝获得的能量大小，一脉一滴条件下，一个脉冲周期内焊丝获得能量越多，焊丝熔化量越大，熔滴直径越大；反之则越小. 一个脉冲周期内焊丝获得的能量计算式为

$$E = \sum_{t=a}^{b} \eta U_t I_t t \tag{4}$$

式中：a 和 b 为单个脉冲周期的开始和结束的时间；

η为焊接输出能量提供给焊丝的百分比；U_t为焊接电压；I_t为焊接电流；t为采样数据点的时间间隔. 脉冲频率越高，基值时间越短，由于峰值时间保持恒定，因此当脉冲频率较高时，在一定的时间内，峰值时间占比大，焊机输出功率高，但是对于单个脉冲周期，由于基值时间的大幅缩短，该周期内的总能量减小，因此熔滴直径也就减小了，如图 9(b) 所示.

熔滴的过渡频率和直径大小影响焊接熔池的稳定性. 在焊接速度一定的条件下，增大送丝速度或者焊接电流，可以减小熔滴尺寸，有利于仰焊位置的熔滴过渡，但是会使焊层厚度增加、组织和性能降低，还会使基值时间减少、熔池过大，造成立焊位置熔池流淌等问题；减小送丝速度或焊接电流，可以增加基值时间，有利于立焊和仰焊位置的熔池稳定，降低焊层厚度，保证组织性能，但是会使熔滴尺寸增加，不利于仰焊位置熔滴过渡，甚至出现过渡失败的情况.

在工艺试验中，首先确定能够保证熔滴过渡的最小送丝速度，然后在平焊到立焊的焊接过程采用较高的焊接速度和送丝速度，获得较高的焊接效率. 在立焊到仰焊的焊接过程降低送丝速度以保证熔池的稳定，降低焊接速度以维持焊层厚度一致，但是仰焊位置的送丝速度要能够保证熔滴的稳定过渡.

2.2.3 CTWD 对熔滴过渡的影响

熔滴要克服重力运动到熔池，熔滴过渡的路径越短，越有利于熔滴的过渡，但是由于电弧的自调节作用，压低焊枪对于电弧长度的影响不大，对于缩短熔滴过渡路程的影响有限，但是压低焊枪可以减小熔滴直径，提高焊接电流，从而对熔滴过渡产生积极的影响. 图 10 为 CTWD 由 20 mm 位置逐渐下降为 10 mm 过程的电流和电压曲线，图 11 为焊枪压低前后熔滴在开始形成到熔滴脱离焊丝所受

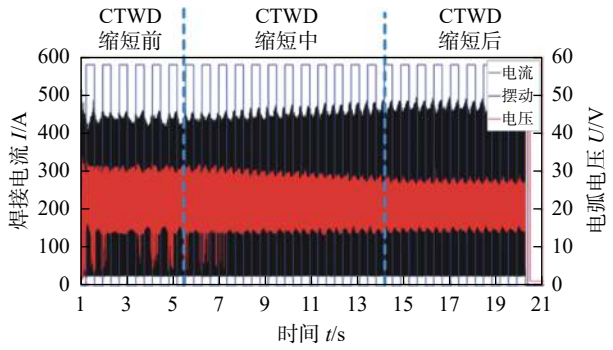

图 10 CTWD 变化前后电压电流

Fig. 10 Voltage and current change diagram before and after CTWD change

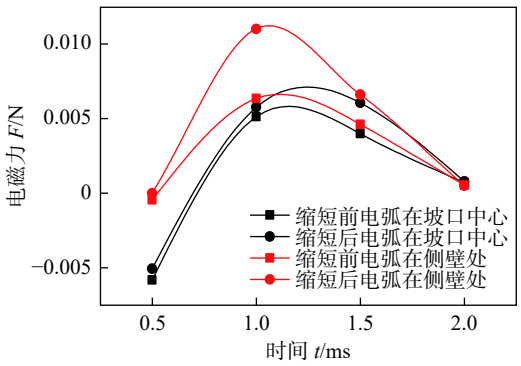

图 11 熔滴所受电磁力

Fig. 11 Electromagnetic force on the droplet

电磁力，从图中可以看出熔滴开始形成阶段，熔滴所受的电磁力为阻碍熔滴过渡的力，压低焊枪后阻碍熔滴过渡的力有所降低，阻碍熔滴过渡的力的作用时间有所减少. 随着焊枪的压低，电磁力转变为促进熔滴过渡的力，促进熔滴过渡的力有所提高，促进熔滴过渡的力的作用时间有所增加. 并且由于焊接电流在侧壁时的变化较大，因此焊枪压低后，侧壁位置电磁力的增加幅度较大.

由于熔滴过渡过程中熔滴的密度基本不变，所以熔滴所受的重力与熔滴直径直接相关. 分别取焊枪压低前后焊枪在坡口中心以及侧壁各 10 个熔滴，计算熔滴直径的平均值，绘制成图 12. 从图中可以看出，随着 CTWD 的缩短，焊枪在侧壁以及坡口中心时熔滴直径减少，因此熔滴所受的重力减小，仰焊时重力为阻碍熔滴过渡的力，重力的减少有利于熔滴的过渡.

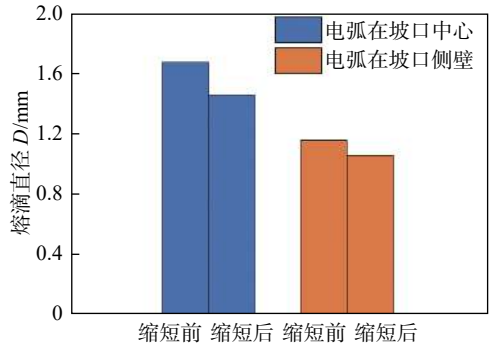

图 12 熔滴直径

Fig. 12 Droplet diameter

熔滴过渡行为由熔滴所受的合外力决定，作用在熔滴上的重力和等离子流力的数量级均小于电磁力，因此焊接过程中熔滴的过渡行为主要受电磁力的影响. 熔滴脱离焊丝时所获得的初速度为

$$V=\sqrt{\sum_{t=c}^{d}\frac{2F_{zt}S}{m_t}} \tag{5}$$

式中: F_{zt}为熔滴所受的合力; m_t为熔滴的质量; S为熔滴形成到脱离焊丝的位移; c, d 分别为熔滴开始生成和熔滴脱离焊丝的时间. 由于焊枪压低后, 熔滴所受促进熔滴过渡的力增加, 阻碍熔滴过渡的的力减少, 且熔滴的质量有所所降低, 因此熔滴可以获得较大的初速度, 有利于熔滴过渡.

在全位置焊接过程中, 焊接专机运动到仰焊位置时, 适当的压低焊枪, 有利于熔滴过渡的完成.

3　结论

(1) 在平焊到立焊的过程, 适当地提高弧长修正系数可以获得稳定无飞溅电弧, 增加对侧壁的热输入. 但是进入仰焊位置后, 应该降低弧长修正系数、采用短弧焊接, 以有效控制熔滴的落点位置, 保证良好的焊缝成形.

(2) 送丝速度越大, 熔滴直径越小、过渡频率越高; 相同的送丝速度下, 焊枪在坡口中心的熔滴过渡直径大于焊枪在坡口侧壁时的熔滴过渡直径. 工艺试验中需要确定能够保证熔滴在仰焊位置过渡的最小送丝速度.

(3) 电磁力促进熔滴过渡的时间随着 CTWD 的缩短逐渐增加, 促进熔滴过渡的力峰值也有所提高; 阻碍熔滴过渡的力随着 CTWD 的缩短有所降低, 阻碍熔滴过渡的力的作用时间有所减少, 降低焊枪有利于窄间隙仰焊的熔滴过渡.

参考文献

[1] 陈树君, 卢振洋, 任福深, 等. 管道全位置自动焊机的专用电源及焊接工艺 [J]. 焊接学报, 2009, 30(2): 13 − 16.
Chen Shujun, Lu Zhenyang, Ren Fushen, *et al*. Special welding machine and welding process for all position automatic pipeline welding[J]. Transactions of the China Welding Institution, 2009, 30(2): 13 − 16.

[2] 丁玉明, 汪雄飞, 刘霞, 等. NiCrMoV 转子钢窄间隙焊接接头显微组织及力学性能研究 [J]. 上海金属, 2018, 40(1): 8 − 14.
Ding Yuming, Wang Xiongfei, Liu Xia, *et al*. Investigation on the microstructure and mechanical properties of narrow gap welded joint of NiCrMoV rotor steel[J]. Shanghai Metals, 2018, 40(1): 8 − 14.

[3] 杨宽, 高辉, 周灿丰. 基于 Fluent 的窄间隙 TIG 焊枪结构优化设计 [J]. 焊接, 2022(8): 39 − 43.
Yang Kuan, Gao Hui, Zhou Canfeng. Optimization design of narrow gap TIG welding torch's structure based on Fluent[J]. Welding & Joining, 2022(8): 39 − 43.

[4] 郑韶先, 李晔楠, 史伟, 等. 超窄间隙焊接 Q235/1Cr18Ni9Ti 异种钢接头组织及力学性能 [J]. 焊接学报, 2019, 40(8): 38 − 43.
Zheng Shaoxian, Li Huanan, Shi Wei, *et al*. Microstructures and mechanical properties of welding joint of Q235/1Cr18Ni9Ti dissimilar steel with ultra-narrow-gap[J]. Transactions of the China Welding Institution, 2019, 40(8): 38 − 43.

[5] 冯靖, 武少杰, 高洪明, 等. 基于熔池受力的全位置 STT 打底焊分段工艺 [J]. 焊接, 2022(2): 1 − 5.
Feng Jing, Wu Shaojie, Gao Hongming, *et al*. Subsection process of all-position STT backing welding based on the force in molten pool[J]. Welding & Joining, 2022(2): 1 − 5.

[6] 贾传宝, 杜永鹏, 武传松, 等. 厚板窄间隙磁控电弧 TIG 焊接自动控制系统设计 [J]. 华南理工大学学报(自然科学版), 2017, 45(9): 40 − 46.
Jia Chuanbao, Du Yongpeng, Wu Chuansong, *et al*. Design of an automatic control system for magnetic controlled narrow-gap TIG arc welding of thick plates[J]. Journal of South China University of Technology(Natural Science Edition), 2017, 45(9): 40 − 46.

[7] 张阳, 吕小青, 徐连勇, 等. 工件倾角对脉冲 MAG 焊接熔池形态和焊缝尺寸的影响 [J]. 焊接学报, 2019, 40(10): 36 − 42.
Zhang Yang, Lü Xiaqing, Xu Lianyong, *et al*. Effect of workpiece inclination on weld pool shape and weld forming in pulsed MAG welding[J]. Transactions of the China Welding Institution, 2019, 40(10): 36 − 42.

[8] 徐刚, 张天雷, 何林基, 等. 窄间隙摆动电弧数值模拟 [J]. 轻工机械, 2021, 39(3): 54 − 58.
Xu Gang, Zhang Tianlei, He Linji, *et al*. Numerical simulation of welding arc with narrow gap[J]. Light Industry Machinery, 2021, 39(3): 54 − 58.

[9] 徐望辉, 林三宝, 杨春利, 等. 摆动电弧窄间隙 GMAW 熔滴过渡规律 [J]. 焊接学报, 2017, 38(2): 109 − 114.
Xu Wanghui, Lin Sanbao, Yang Chunli, *et al*. Study on droplet transfer of swing arc narrow gap GMAW[J]. Transactions of the China Welding Institution, 2017, 38(2): 109 − 114.

[10] 王定洲, 陈刚, 张宇, 等. 空间焊接位置对熔滴过渡的影响 [J]. 江苏科技大学学报(自然科学版), 2018, 32(5): 633 − 636.
Wang Dingzhou, Chen Gang, Zhang Yu, *et al*. Effect of spatial welding positions on molten droplet transfer[J]. Journal of Jiangsu University of Science and Technology(Natural Science Edition), 2018, 32(5): 633 − 636.

[11] Alireza D T. Neutralizing the effect of the angle variations on the drop detachment in automatic GMAW system[J]. The International Journal of Advanced Manufacturing Technology, 2010, 54(1-4): 123 − 137.

第一作者: 刘文吉，博士，高级实验师；主要从事焊接自动化、焊接过程质量控制方面研究；Email: liuwenji1981@126.com.

（编辑：　张基隆）

tain component diffusion between the brazing coating and steel substrate. And the thickness of narrowest diffusion area is about 100 μm. When the WC content is lower than 25wt.%, the brazing coating has better wettability on the steel substrate. The internal denseness of the coating stays in high level. Meanwhile, the minimum porosity in the composite coating can be kept at 1.08%.

Highlights: (1) The nickel/tungsten carbide superhard composite coatings on austenitic stainless steel surfaces by vacuum brazing coating method for hydraulic machinery overflow components have been successfully prepared.
(2) Wettability performance of brazing filler metals and interfacial reaction and diffusion of composite brazing coatings are revealed.

Key words: brazing; composite coating; nickel/tungsten carbide interface; interface microstructure; wettability

Vacuum brazing TC4 titanium alloy / 316L stainless steel with $Ti_{43.76}Zr_{12.50}Cu_{37.49-x}Ni_{6.25}Co_x$ amorphous filler metals

HAN Wenqian, DONG Honggang, MA Yueting, LI Peng, WU Baosheng, ZHANG Liangliang(Dalian University of Technology, Dalian, 116024). pp 47-57

Abstract: Ti-Zr-Cu-Ni-Co amorphous filler metals were designed and prepared for vacuum brazing of TC4 titanium alloy to 316L stainless steel according to the dual-cluster model. The effect of Co content in filler metals on the microstructure, mechanical properties and fracture behavior of brazed joints was investigated. The results showed that the cross section of brazed joint could be divided into TC4/diffusion zone I/brazing seam center zone II/interface zone III/316L. The typical interfacial microstructure of the brazed joints was TC4/β-Ti + Ti_2Cu/$(Ti, Zr)_2(Cu, Ni)$ + Ti_2Cu + $Ti_2(Cu, Ni)$ + TiFe/$(Fe, Cr)_2Ti$ + α-(Fe, Cr) + τ + γ -(Fe, Ni) + σ/316L. The shear strength of brazed joints first increased, then decreased and then increased with the increase of Co content. The maximum shear strength of 310 MPa was obtained at 1.56% Co. When Co element was not added, brazed joints fractured in the center of the brazing seam (zone II). And when the Co content was 1.56 ~ 6.24%, brazed joints fractured near the interface zone (zone III) of 316L base metal. The fracture mode was typical cleavage fracture.

Highlights: (1) Ti-Zr-Cu-Ni-Co amorphous filler metals were designed and prepared based on the dual-cluster model.
(2) The effect of Co content in filler metals on the microstructure, mechanical properties and fracture behavior of brazed joints was elucidated.

Key words: vacuum brazing; amorphous filler metal; titanium alloy/stainless steel dissimilar metal; microstructure; shear strength

Influence factors and control methods of droplet transfer in narrow gap P-GMAW overhead welding position

LIU Wenji, XIAO Yu, YANG Jiasheng, ZHU Pengfei(Tiangong University, Tianjin, 300387, China). pp 58-63

Abstract: When conducting narrow gap all position welding of pipelines, welding defects are easy to occur near the overhead welding position, which restricts the quality and efficiency of pipeline construction. Aiming at the problem of poor formation and low reliability of overhead welding position in automatic pipe welding, this paper studies the influence of wire feeding speed, arc length correction, contact nozzle distance to molten pool and other factors on droplet transfer in P-GMAW process. It is found that increasing the arc length correction coefficient can increase the heat input of the arc to the side wall, which can alleviate the problem of poor side wall fusion, but will make the droplet transfer path difficult to control, Therefore, when the welding gun moves to the overhead welding position, short arc welding shall be adopted and the heat input to the side wall shall be supplemented by increasing the side stop time and swing; Increasing the wire feeding speed is conducive to obtaining smaller droplets, higher transfer frequency, reducing the distance between the contact tip and the molten pool, increasing the electromagnetic force and reducing the droplet size, which is more conducive to the transfer of droplets to the molten pool in overhead welding position. The research results have certain guiding significance for the process design of pipe narrow gap welding.

Highlights: This paper Studied the influence of parameters on droplet transfer during narrow gap full position P-GMAW process in pipelines, and the method of controlling welding

parameters to achieve better droplet transfer.

Key words: droplet transfer; Swing arc; MIG welding; Narrow gap welding

Study on sensitization characteristics of TP347H stainless steel welded joints LI Chengan[1], FENG Daochen[1], ZHANG Lin[2], ZHENG Wenjian[1], CHENG Mao[3], LU Xianjing[3], YANG Jianguo[1](1. Zhejiang University of Technology, Hangzhou, 310014, China; 2. CFHI Dalian Nuclear Power and Petrochemical Equipment Co.,Ltd., Dalian 116113, China; 3. Zhejiang Academy of Special Equipment Science, Hangzhou, 310020, China). pp 64-72

Abstract: In order to clarify the sensitization characteristics of TP347H stainless steel welded joints, the welded joints were heat treated at different temperatures, and the changes of sensitization degrees at different temperatures were studied. The results showed that an obvious sensitization trend was observed in the heat-affected zone(HAZ) of welded joints. During the sensitization process, because the binding energy of Nb atoms on the grain boundary is higher than that of Cr atoms, coarse primary niobium carbon compounds are formed first, and then fine secondary niobium carbon compounds are formed. When the temperature is kept at 700 ℃, the sensitization degree of the HAZ of the welded joint shows a trend of first increasing and then decreasing. When the temperature reaches 800 ℃ and above, heat treatment no longer increases the sensitization degree of the HAZ of the joint. Comparing with the sensitization characteristics of F347H joints with 21 000 h in the actual production line, it is confirmed that the sensitization limit can be reached by holding the welded joints of TP347H at 650 ℃ for 100 h. The reason is that the content of Nb is several times that of C, most of C combines with Nb to form NbC, and the diffusion of C in the grain has been fully combined with Cr. The resulting sensitization reaches an equilibrium state.

Highlights: (1) Confirmed that TP347H stainless steel welded joint was heat treated at 650 for 100h can reach the sensitization limit.

(2) In the process of sensitization, because the binding energy of Nb atoms on the grain boundary is higher than that of Cr atoms, the coarse niobium carbon compound will be formed first, and then the fine niobium carbon compound will be formed.

(3) When the TP347H stainless steel welded joint was heat treated at 700 ℃, the sensitization degree in the theat affected zone of the welding joint shows a trend of increasing first and then decreasing.

Key words: TP347H stainless steel; sensitization; welded joint; heat treatment; corrosion resistance

Numerical simulation of the influence of thickness of cladding material on stress and strain of welded joint of stainless steel composite plate FENG Yulan, WU Zhisheng, SUN Zhiyu(Taiyuan University of Science and Technology, Taiyuan, 030024, China). pp 73-82

Abstract: GTAW technology has been used to fabricate welded connections on composite plates consisting of 304 and Q355 materials. Base material thickness was 13 mm, while cladding material thicknesses ranged from 0.3 mm to 2.0 mm. The influence of different thicknesses of cladding material on the stress and strain of 304/Q355 composite plate welded joint was analyzed by numerical simulation method, and the evolution characteristics of residual stress and strain during welding of stainless steel composite plate with different thicknesses of cladding material were revealed. The results show that the X-ray diffraction test results are in good agreement with the numerical simulation results. With the increase of the thickness of the cladding material, the maximum residual stress value of the welded joint section of 304/Q355 composite plate gradually decreases, and the width of the residual stress zone gradually increases. During the welding process from the base weld to the transition weld, the stress concentration zone gradually shrinks to the transition weld zone. Finally, the highest stress concentration area is located in the weld zone of the transition layer, and the maximum stress value is close to the yield strength of the material. In addition, the deformation after welding increases with the increase of the thickness of the cladding material, and the deformation of the composite plate with the thickness of the cladding material 2.0 mm is about 2 mm higher than that of the composite plate with the thickness of the cladding material 0.3 mm, and the direction of the largest deformation is the direction of the weld thickness.